Journal of Sound and Vibration 541 (2022) 117318

Contents lists available at ScienceDirect

Journal of Sound and Vibration

journal homepage: www.elsevier.com/locate/jsvi

Closed-form solutions for attenuation peaks and band boundaries of general monocoupled systems

Abhigna Bhatt [a], Arnab Banerjee [a,*], Sondipon Adhikari [b,1]

[a] Department of Civil Engineering, Indian Institute of Technology Delhi, India
[b] James Watt School of Engineering, The University of Glasgow, Glasgow, UK

ARTICLE INFO

Keywords:
Dispersion relation
Negative mass
Negative stiffness
Inertial amplifier
Attenuation characteristic

ABSTRACT

The unit cells connected periodically at a single node with only one degree of freedom is called a monocoupled system. Dispersion relations for such systems are studied widely; however, the analytical solution for salient features of the attenuation band, such as the number of peaks in a band and band merging, have been relatively unexplored. In this paper, a general theory for obtaining the attenuation characteristics of the general monocoupled system from the roots and poles of the rational polynomial of the dispersion relation is developed. The uniqueness of the developed rational polynomial method is that it can predict the attenuation peaks and the possibility of multiple peaks in an attenuation band due to coupling between the different band formation mechanisms in addition to standard band boundaries. The most general monocoupled system has been conceptualized by combining the three mechanisms, namely inertial amplifier, effective negative mass, and effective negative stiffness. This general system is named Inertial Amplifier Negative Mass Negative Stiffness (IANMNS). This designed monocoupled system degenerates into other seven subsystems as special cases, such as the Inertial Amplifier Negative Stiffness (IANS), the Inertial Amplifier Negative Mass (IANM), the Negative Mass Negative Stiffness (NMNS), the Inertial Amplifier (IA), the Negative Stiffness (NS), the Negative Mass (NM) and the Monoatomic system. The closed-form expressions for the peaks in attenuation level and bounds in terms of nondimensional frequency ratio and other governing parameters such as the inertial mass ratio, mass ratios of resonators one (embedded in main chain mass) and two (embedded in inertial mass), frequency ratios of resonators one and two, and angular parameter are derived for the IANMNS and all the other seven subsystems. The conditions for obtaining the double peaks and band merging are defined analytically.

1. Introduction

A periodic system, in which unit cells are connected with their neighboring units via a single degree of freedom (dof) at a single coordinate, is called a monocoupled system. A mono-coupled periodic system can be conceptualized as a series of spring–mass lattice systems. Additionally, a monocoupled system has only one coupling dof linked with the adjacent element; therefore, the existence of only two distinct opposite directional waves is feasible. Moreover, both of these waves have reciprocal wavenumber (κ) corresponding to a particular free wave frequency (ω) [1]. The relation between the wavenumber (κ) and free wave frequency

* Corresponding author.
E-mail addresses: Abhigna.Sandipkumar.Bhatt@civil.iitd.ac.in (A. Bhatt), abanerjee@iitd.ac.in (A. Banerjee), Sondipon.Adhikari@glasgow.ac.uk (S. Adhikari).
[1] Professor of Engineering Mechanics.

https://doi.org/10.1016/j.jsv.2022.117318
Received 15 March 2022; Received in revised form 1 September 2022; Accepted 20 September 2022
Available online 26 September 2022
0022-460X/

(ω) is called dispersion relation, which can be determined with the help of Block–Floquet theorem [2]. Wave propagation through periodic monocoupled systems has been a topic of investigation for long; due to its ability to create frequency band gaps [3–7] consisting of attenuation band and propagation band. It has wide range of applications such as: noise reduction in helicopter cabin induced by vibration of gearbox using periodic struts [8], vibration absorbers in 1D lumped mass model [9], vibration suppression using chiral lattice [10], etc. Attenuation band is a range of frequencies of which a wave decays spatially. Free waves in a system, scatters due to the periodic interference, this phenomenon is known as Bragg scattering and is considered to be one of the band formation mechanisms of the mono-coupled systems [11–15].

With the discovery of the concept of the local resonance [16,17], the sub-wavelength bandgaps are possible to be achieved exploiting the hybridization mechanism between dispersion and resonance [18–21]. The characterization of local resonance bandgap is primarily comprehended by evaluating the effective properties of the unit cell for respective frequency range. For example, the existence of the negative effective mass in a mass in mass resonator [22–24] or effective negative stiffness in a Helmholtz resonator [25–27] near attenuation peaks were reported. These extreme properties in a resonating metamaterial results in an attenuation band near the natural frequency of the embedded resonator [28,29]. Embedding a resonator inside a unit of metamaterial will yield a narrow band near resonating frequency [24,30]. Further, an inertial amplifier mechanism [31–34] has been introduced, which amplifies the effective mass of the system by a special mechanism using rigid link [35–37]. Unlike the effective mass of the mass-in-mass metamaterial, the inertial amplifier alters the effective inertia of the system in a constant amount throughout the frequency spectrum. This inertial amplifier system yields an attenuation band having peak/s, which increases the attenuation level. Moreover, the double peaks in attenuation band due to resonance coupling and band merging have been obtained in the recent state of art [38,39]. Often, double peaks in stopband results in a high attenuation level for a wide frequency range [39,40], which eradicates the primary shortcoming of mass-in-mass metamaterial that the attenuation level within the band is very low for significant parts of the attenuation band [32].

Motivated by these remarkable features of the monocoupled systems, researchers studied the coupling of various mechanisms such as effective negative mass, and stiffness [41–43] and a mass in mass resonator with IA to obtain double peak in attenuation band [40], for obtaining a wider attenuation band. Expressions of the bounding frequencies were reported in the literature [44–46], and the dispersion diagram can be obtained in the frequency domain applying Bloch–Floquet's theory. However, the condition for the double peak phenomenon and the close form analytical expression for the exact location of the peaks in the attenuation band were still missing from the state of the art.

A generalized monocoupled system consisting of three mechanisms, namely mass in mass resonator, inertial amplifier, and Helmholtz resonator, has been developed to bridge the mentioned research gap. This proposed generalized system can be reduced to seven monocoupled subsystems by assuming corresponding mass to zero, as depicted in Fig. 2. Further, a general framework implementing rational polynomial is developed in this paper from which the closed form expressions for the position of attenuation peaks and bounding frequencies of propagation band can be identified for any undamped monocoupled system. Damping is an inherent property of any material; however, its decaying nature is perceivable in time domain response. Wave attenuation is a phenomenon in the spatial domain; therefore, inherent small material damping does not significantly affect the characteristics of the bands, including band boundaries and attenuation peaks. Although a notable alteration in band characteristics may be observed for the inclusion of high viscous damping and metadamping could also be noticed in that case [47]. From the roots of the denominator of the rational polynomial, the position of the peaks in the attenuation band and the possibility of double peaks can be identified. The novelty of the paper lies in realizing the monocoupled system, which can act as a generalized system for the majority of the monocouple systems existing in the literature, and the proposition of a rational polynomial based approach to predict the peaks and bounds of the attenuation band. Moreover, the effect on attenuation characteristics has been conceptualized by performing a parametric variation of the governing parameters. It is noteworthy that the developed theory is directly applicable only for the undamped monocoupled systems.

2. The generalized mono-coupled system: Conceptualization

In this paper, a generalized monocoupled system has been introduced, which is a combination of systems with an inertial amplifier, negative mass, and negative stiffness. Fig. 2(a) represents a unit metamaterial cell in periodic arrangement of monocoupled system with combined inertial amplifier, negative mass, and negative stiffness.

This generalized system will be called as the Inertial Amplifier Negative Mass Negative stiffness (IANMNS) system. Here the main chain has mass M and stiffness K. The first resonator with mass m_1 and stiffness k_1 is connected directly to main mass M. The mass M has another mass m_a attached with rigid links to act as an inertial amplifier. The vertical barriers shown in Fig. 1(a), are placed to confine the motion of inertial mass m_a in only vertical direction. The second resonator with mass m_2 and stiffness k_2 is connected to mass m_a. So here, four different masses are there in a single representative unit cell. This generalized IANMNS system can be reduced to seven subsystems, as illustrated in Figs. 2(b–h).

2.1. Equation of motion of each mass

The dynamic stiffness matrix can be constructed using governing equations of motion and compatibility equations of the system. The degrees of freedom of IANMNS system are shown in Fig. 1(b). The governing equations of motion at nodes 2 and 7 of resonator mass embedded in base chain can be written as

$$\text{node 2:} \quad m_1\ddot{u}_2 + k_1\left(u_2 - u_1\right) = 0 \tag{1}$$

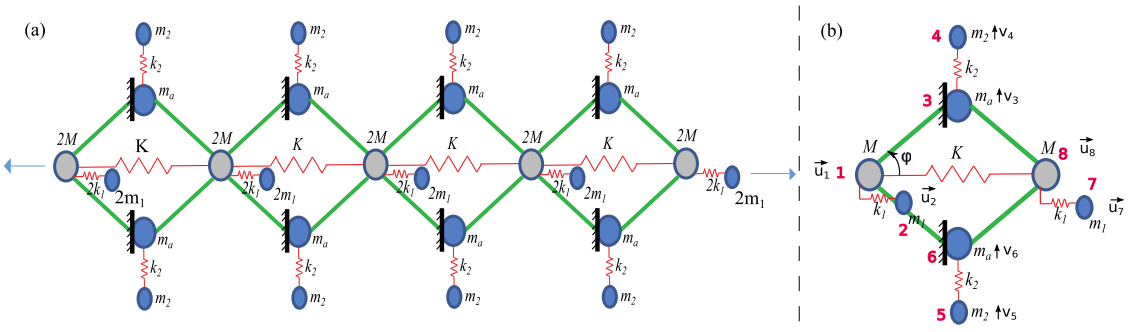

Fig. 1. (a) Periodically connected infinitely long chain of IANMNS system, (b) Nodal degrees of freedom of IANMNS system.

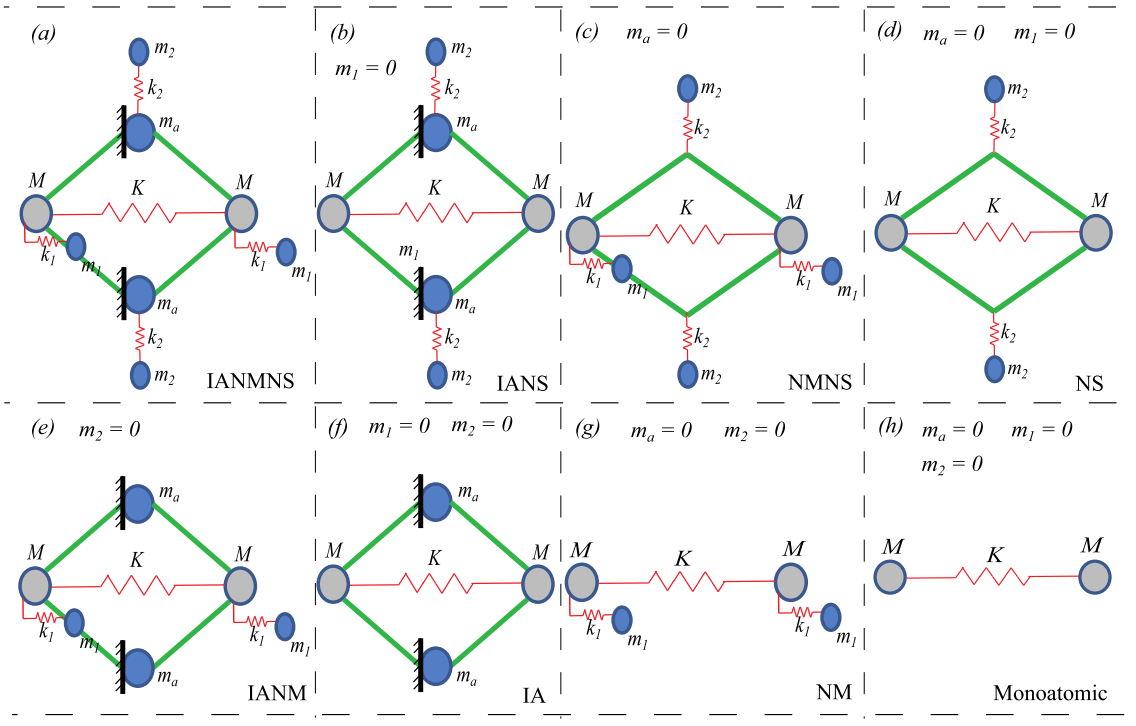

Fig. 2. (a) Generalized monocoupled system Inertial Amplifier Negative Mass Negative Stiffness (IANMNS) (b) Inertial Amplifier Negative Stiffness (IANS) system obtained by considering $m_1 = 0$, (c) Negative Mass Negative Stiffness (NMNS) system obtained by considering $m_a = 0$, (d) Negative Stiffness (NS) system obtained by considering $m_a = 0$ and $m_1 = 0$, (e) Inertial Amplifier Negative Mass (IANM) system obtained by considering $m_2 = 0$, (f) Inertial Amplifier (IA) system obtained by considering $m_1 = 0$ and $m_2 = 0$, (g) Negative Mass (NM) system obtained by considering $m_a = 0$ and $m_2 = 0$, (h) basic monoatomic system obtained by considering $m_a = 0$, $m_1 = 0$ and $m_2 = 0$.

$$\text{node 7:} \quad m_1\ddot{u}_7 + k_1\left(u_7 - u_8\right) = 0 \tag{2}$$

Similarly at nodes 4 and 5, the governing equations of motion of resonators embedded in mass (m_a) connected with rigid links can be written as

$$\text{node 4:} \quad m_2\ddot{v}_4 + k_2\left(v_4 - v_3\right) = 0 \tag{3}$$

$$\text{node 5:} \quad m_2\ddot{v}_5 + k_2\left(v_5 - v_6\right) = 0 \tag{4}$$

The nodes 1 and 8, as well as nodes 3 and 6 have rigid links attached to them, which can be modeled in terms of force (f_n) and the governing equations of nodes 1, 3, 6 and 8 can be written as

$$\text{node 1:} \quad M\ddot{u}_1 + K\left(u_1 - u_8\right) + k_1\left(u_1 - u_2\right) = 2\,f_n\cos\phi \tag{5}$$

$$\text{node 8:} \quad M\ddot{u}_8 + K\left(u_8 - u_1\right) + k_1\left(u_8 - u_7\right) = 2\,f_n\cos\phi \tag{6}$$

$$\text{node 3:} \quad m_a \ddot{v}_3 + k_2 \left(v_3 - v_4\right) = 2 f_n \sin\phi \tag{7}$$

$$\text{node 6:} \quad m_a \ddot{v}_6 + k_2 \left(v_6 - v_5\right) = 2 f_n \sin\phi \tag{8}$$

Here, $(\ddot{\bullet})$ denotes two time derivative so $(\ddot{\bullet}) = -\omega^2 (\bullet)$ can be written.

2.2. Compatibility equation

The compatibility equations of nodes 1, 3, 6 and 8 can be determined by kinematics of rigid links as follows

$$\text{Displacement at node 3:} \quad v_3 = \frac{u_8 - u_1}{2\tan\phi} \tag{9}$$

$$\text{and} \quad \text{Displacement at node 6:} \quad v_6 = \frac{u_1 - u_8}{2\tan\phi} \tag{10}$$

Using equations of motion of node 3, 4, 5 and 6 (Eq. (7), Eq. (3) and Eq. (4), Eq. (8)); and compatibility equations of displacements at node 3 and node 6 (Eq. (9) and Eq. (10)), the force in rigid links can be calculated as

$$f_n = \frac{1}{4\tan\phi\,\sin\phi}\left(-m_a\,\omega^2 + k_2 - \frac{{k_2}^2}{-m_2\,\omega^2 + k_2}\right)\left(u_8 - u_1\right) \tag{11}$$

substituting Eq. (11) into the term $(2 f_n \cos\phi)$ present in governing equations of nodes 1 and 8 can be written as

$$l_n = 2 f_n \cos\phi = \frac{1}{2\tan^2\phi}\left(-m_a\,\omega^2 + k_2 - \frac{{k_2}^2}{-m_2\,\omega^2 + k_2}\right)\left(u_8 - u_1\right) \tag{12}$$

2.3. Construction of Dynamic Stiffness Matrix

The Dynamic Stiffness matrix (D_y) can be obtained as

$$\mathbf{D}_y = -\omega^2\,\mathbf{M} + \mathbf{K} + \mathbf{L} \tag{13}$$

Where, the stiffness matrix (**K**) and mass matrix (**M**) can be formulated using equations of motion at node 1, 2, 7 and 8 (Eq. (5), Eq. (1), Eq. (2) and Eq. (6)). Moreover, the corresponding response vector **u** is vector of displacements at nodes 1, 2, 7 and 8

$$\mathbf{K} = \begin{bmatrix} K + k_1 & -k_1 & 0 & -K \\ -k_1 & k_1 & 0 & 0 \\ 0 & 0 & k_1 & -k_1 \\ -K & 0 & -k_1 & K + k_1 \end{bmatrix}, \quad \mathbf{M} = \begin{bmatrix} M & 0 & 0 & 0 \\ 0 & m_1 & 0 & 0 \\ 0 & 0 & m_1 & 0 \\ 0 & 0 & 0 & M \end{bmatrix} \tag{14}$$

$$\mathbf{u} = \begin{pmatrix} u_1 & u_2 & u_7 & u_8 \end{pmatrix}' \tag{15}$$

Further, incorporating Eq. (12), the forces at nodes 1 and 8 due to rigid links can be written in matrix form as

$$\mathbf{L} = \begin{bmatrix} l_n & 0 & 0 & -l_n \\ 0 & 0 & 0 & 0 \\ 0 & 0 & 0 & 0 \\ -l_n & 0 & 0 & l_n \end{bmatrix} \tag{16}$$

The dynamic stiffness matrix is obtained as

$$\mathbf{D}_y = \begin{bmatrix} -\omega^2 M + K + k_1 + l_n & -k_1 & 0 & -K - l_n \\ -k_1 & -\omega^2 m_1 + k_1 & 0 & 0 \\ 0 & 0 & -\omega^2 m_1 + k_1 & -k_1 \\ -K - l_n & 0 & -k_1 & -\omega^2 M + K + k_1 + l_n \end{bmatrix} \tag{17}$$

By necessary matrix manipulations the condensed Dynamic Stiffness matrix (D_{yc}) for responses at node 1 and node 8 is obtained as

$$\mathbf{D}_{yc} = \begin{bmatrix} -\omega^2 M + K + k_1 + \frac{{k_1}^2}{\omega^2 m_1 - k_1} + l_n & -K - l_n \\ -K - l_n & -\omega^2 M + K + k_1 + \frac{{k_1}^2}{\omega^2 m_1 - k_1} + l_n \end{bmatrix} \tag{18}$$

Receptance matrix of the IANMNS system can be calculated by taking inverse of the condensed dynamic stiffness matrix D_{yc}

$$\boldsymbol{\alpha}_R = \mathbf{D}_{yc}^{-1} = \begin{bmatrix} \alpha_{LL} & \alpha_{LR} \\ \alpha_{RL} & \alpha_{RR} \end{bmatrix} \tag{19}$$

Where

$$\alpha_{LL} = \frac{1}{|\mathbf{D}_{yc}|}\left(-\omega^2 M + K + k_1 + \frac{{k_1}^2}{\omega^2 m_1 - k_1} + l_n\right) \tag{20}$$

$$\text{and} \quad \alpha_{LR} = \frac{1}{|\mathbf{D}_{\mathbf{yc}}|}\left(K + l_n\right) \tag{21}$$

$$\text{and} \quad |\mathbf{D}_{yc}| = \left(-\omega^2 M + K + k_1 + \frac{{k_1}^2}{\omega^2 m_1 - k_1} + l_n\right)^2 - \left(K + l_n\right)^2 \tag{22}$$

Moreover, because of symmetric representative unit cell, the receptance matrix will have [48]

$$\alpha_{RR} = \alpha_{LL} \tag{23}$$

and due to symmetric dynamic stiffness matrix the receptance matrix will also be the symmetric matrix so

$$\alpha_{RL} = \alpha_{LR} \tag{24}$$

Following this method, the receptance matrix can be formulated for all the seven subsystems by assigning zero to the suitable masses as per given in Figs. 2(b–h).

3. A general theory of attenuation characteristics in monocoupled system

For the unit cell of any monocoupled system, the force displacement relationship can be demonstrated by a receptance matrix as follows [48]

$$\begin{Bmatrix} d_L \\ d_R \end{Bmatrix} = \begin{bmatrix} \alpha_{LL} & \alpha_{LR} \\ \alpha_{RL} & \alpha_{RR} \end{bmatrix} \begin{Bmatrix} f_L \\ f_R \end{Bmatrix} \tag{25}$$

Further, As per Bloch theorem [2], the relation between left and right displacement as well as force can be written as

$$\begin{aligned} d_R &= e^{i\kappa} d_L \\ f_R &= -e^{i\kappa} f_L \end{aligned} \tag{26}$$

Where, κ is a propagation constant. solving Eqs. (25) and (26), the dispersion relation can be explained as

$$\cos(\kappa) = \frac{\alpha_{LL} + \alpha_{RR}}{2\,\alpha_{LR}} \tag{27}$$

Further, using Eqs. (23), (24) and (27), the dispersion relation for the symmetric system can be written as

$$\cos(\kappa) = \frac{\alpha_{LL}}{\alpha_{LR}} \tag{28}$$

As the components of receptance matrix are functions of square of frequency, the general statement for any monocoupled system can be written as

$$\cos(\kappa) = g(\omega^2) = x \tag{29}$$

Now,

$$\begin{aligned} e^{i\kappa} + e^{-i\kappa} &= 2x \\ e^{2i\kappa} + 1 &= 2x\,e^{i\kappa} \\ e^{2i\kappa} - 2x\,e^{i\kappa} + 1 &= 0 \end{aligned} \tag{30}$$

Let $A = e^{i\kappa}$, from Eq. (30)

$$A = x \pm \sqrt{x^2 - 1} \tag{31}$$

Let, solution $\kappa = \alpha + i\beta$, So $\ln A = -\beta + i\alpha$. It is useful to note here that the value of β defines the level of attenuation and α defines the phase of propagating wave. When, $x^2 > 1$, A is real, So when

$$\begin{aligned} &A < 0 \rightarrow \ln A = \ln|A| + i\pi \rightarrow \alpha = \pi \;\&\; \beta = -\ln A \rightarrow \textit{Attenuation} \\ &A > 0 \rightarrow \ln A = \ln|A| + i0 \rightarrow \alpha = 0 \;\&\; \beta = -\ln A \rightarrow \textit{Attenuation} \end{aligned} \tag{32}$$

But when $x^2 < 1$, A is complex. Now, let $x = \cos(\delta)$ so the following can be derived from Eq. (31)

$$A = e^{i\kappa} = e^{i(\alpha + i\beta)} = \cos(\delta) + i\sin(\delta) \rightarrow \alpha = \delta = \cos^{-1}(x) \;\&\; \beta = 0 \rightarrow \textit{Propagation} \tag{33}$$

From Eqs. (32) and (33), it can be concluded that in case of monocoupled systems, the wave will be purely propagating (Fig. 3(a)) or attenuating (Fig. 3(b)) because the wave number cannot have simultaneous non zero imaginary and real values. The simultaneous

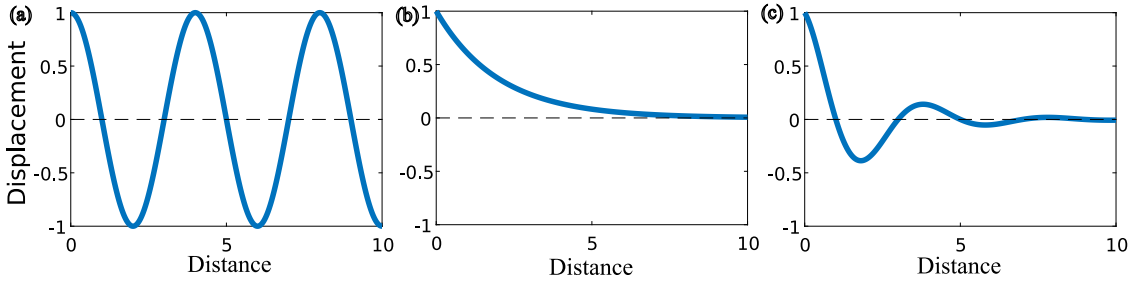

Fig. 3. Displacement patterns for different types of responses (a) pure propagation (b) pure attenuation (c) fluctuating attenuation.

non zero imaginary and real values will cause fluctuating attenuation (Fig. 3(c)), which is impossible in the case of monocoupled systems. Any monocoupled system can be generalized in terms of effective mass (M_{eff}) and effective stiffness (K_{eff}), by comparing it to the mono-atomic chain given in Fig. 2(h). So, the generalized dispersion equation can be obtained as [7]

$$\cos(\kappa) = 1 - \frac{\omega^2 M_{eff}}{K_{eff}} \tag{34}$$

Here, the effective mass and stiffness are also the functions of ω^2. The rational polynomial equation for dispersion relation of any monocoupled system can be obtained as

$$g(\omega^2) = 1 + \frac{R(\omega^2)}{Q(\omega^2)} \tag{35}$$

From the roots and poles of rational polynomial Eq. (35), the salient features of band structure like peak in attenuation and bounding frequencies can be obtained. First, the peaks in the attenuation band occur when $g(\omega^2) \to \infty$, which exists at the poles of Eq. (35), which are the roots of

$$Q(\omega^2) = 0 \tag{36}$$

Further, the propagation boundaries occur when $g(\omega^2) = \pm 1$ (at roots of Eq. (35)), which results in two equations such as

$$1 + \frac{R(\omega^2)}{Q(\omega^2)} = 1 \qquad \to R(\omega^2) = 0 \tag{37}$$

$$1 + \frac{R(\omega^2)}{Q(\omega^2)} = -1 \qquad \to R(\omega^2) + 2Q(\omega^2) = 0 \tag{38}$$

As this monocoupled system is semi definite, the propagation zone will start from zero frequency. So Eq. (37) or Eq. (38) will have zero as its one root, and other roots will define bounds of propagation or attenuation bands.

4. Non-dimensional form and various mono coupled systems

The non-dimensional form of the dispersion relation of the IANMNS system is dependent on the following governing nondimensional parameters:

- $\eta = \frac{\omega}{\sqrt{K/M}}$. Free wave frequency ratio (η) expressed as ratio of free wave frequency (ω) and natural frequency of main chain $\sqrt{K/M}$.
- $\theta = \frac{m_a}{M}$. Inertial mass ratio (θ) defined as the ratio of the inertial mass m_a with the mass at the main chain M.
- $\theta_{r1} = \frac{m_1}{M}$. Mass ratio ($\theta_{r1}$) is defined as the ratio of the mass of resonator embedded in main chain and main mass.
- $\eta_{r1} = \frac{\sqrt{k_1/m_1}}{\sqrt{K/M}}$. Frequency ratio of the resonator one attached to the main chain is defined as ratio of the natural frequency of the first resonator with the natural frequency of the main chain ($\sqrt{K/M}$).
- $\theta_{r2} = \frac{m_2}{M}$. Mass ratio ($\theta_{r2}$) is defined as the ratio of the mass of resonator two (m_2) and main mass M.
- $\eta_{r2} = \frac{\sqrt{k_2/m_2}}{\sqrt{K/M}}$. Frequency ratio of the resonator two is defined as ratio of the natural frequency of the second resonator with the natural frequency of the main chain ($\sqrt{K/M}$).
- $\gamma = \tan^2\phi$. angular parameter γ is the square of a tangent of the angle made by rigid links with x-axis in the anticlockwise direction.

4.1. Peak in attenuation level and bounds of propagation band

For the IANMNS system, the equation of dispersion relation in the form of Eq. (35) is obtained from Eq. (20) and Eq. (28) in nondimensional parameters, where $Q(\eta^2)$ and $R(\eta^2)$ are

$$\begin{aligned} R(\eta^2) &= R_3\eta^6 + R_2\eta^4 + R_1\eta^2 + R_0 \\ \text{and} \quad Q(\eta^2) &= Q_3\eta^6 + Q_2\eta^4 + Q_1\eta^2 + Q_0 \end{aligned} \tag{39}$$

where, the coefficients of equation $R = 0$ are

$$\begin{aligned} R_3 &= -2\,\gamma \\ R_2 &= 2\,\gamma\,{\eta_{r2}}^2 + 2\,\gamma\,\left({\eta_{r1}}^2\theta_{r1} + {\eta_{r1}}^2\right) \\ R_1 &= -2\,\gamma\,\left({\eta_{r1}}^2\theta_{r1} + {\eta_{r1}}^2\right){\eta_{r2}}^2 \\ \text{and} \quad R_0 &= 0 \end{aligned} \tag{40}$$

The coefficients of equation $Q = 0$ are

$$\begin{aligned} Q_3 &= -\theta \\ Q_2 &= {\eta_{r1}}^2\theta + {\eta_{r2}}^2\theta + {\eta_{r2}}^2\,\theta_{r2} + 2\,\gamma \\ Q_1 &= \left(-{\eta_{r2}}^2\theta - {\eta_{r2}}^2\,\theta_{r2} - 2\,\gamma\right){\eta_{r1}}^2 - 2\,\gamma\,{\eta_{r2}}^2 \\ \text{and} \quad Q_0 &= 2\,\gamma\,{\eta_{r1}}^2{\eta_{r2}}^2 \end{aligned} \tag{41}$$

To study the possible number of peaks present in a single attenuation band, roots of any one boundary equation (that is $R = 0$ or $R + 2Q = 0$) and attenuation peak equation (that is $Q = 0$) is necessary. Analytically roots of all three equations can be obtained, however here we have given solution for only two equations i.e. $Q = 0$ and $R = 0$, as closed form solution of $R + 2Q = 0$ is complicated to write for IANMNS system.

The roots of $Q = 0$ are

$$\begin{aligned} q_1 &= \eta_{r1} \\ q_2, q_3 &= \sqrt{\frac{1}{2\,\theta}\left({\eta_{r2}}^2\,\left(\theta + \theta_{r2}\right) + 2\,\gamma \pm \sqrt{\left({\eta_{r2}}^2\,\left(\theta + \theta_{r2}\right) + 2\,\gamma\right)^2 - 8\,{\eta_{r2}}^2\gamma\,\theta}\right)} \end{aligned} \tag{42}$$

It can be concluded from the roots of equation $Q = 0$ that, the root q_1 is obtained from natural frequency of mass in mass resonator and q_2 and q_3 are result of combined effects of inertial amplifier and negative stiffness resonator. As $R_0 = 0$, its first root is $\eta = 0$, which shows the starting of propagation zone. Roots of $R = 0$ are

$$\begin{aligned} r_1 &= 0 \\ r_2 &= \eta_{r2} \\ r_3 &= \sqrt{{\eta_{r1}}^2\theta_{r1} + {\eta_{r1}}^2} = \eta_{r1}\sqrt{(1 + \theta_{r1})} \end{aligned} \tag{43}$$

The roots r_2 and r_3 are boundaries of dispersion diagram. The positions of these roots are such that all three peaks of attenuation can never be in a single attenuation band (proved in Appendix).

Further, by placing zero value to the non required mass into the dynamic stiffness matrix of IANMNS system as per given in Fig. 2; the Q and R equations and their roots corresponding to all obtained systems are obtained in Table 1. Following are the variables name given to the roots according to their reason of existence

$$\xi_1 = \sqrt{\frac{1}{2\,\theta}\left({\eta_{r2}}^2\,\left(\theta + \theta_{r2}\right) + 2\,\gamma - \sqrt{\left({\eta_{r2}}^2\,\left(\theta + \theta_{r2}\right) + 2\,\gamma\right)^2 - 8\,{\eta_{r2}}^2\gamma\,\theta}\right)} \tag{44}$$

$$\xi_2 = \sqrt{\frac{1}{2\,\theta}\left({\eta_{r2}}^2\,\left(\theta + \theta_{r2}\right) + 2\,\gamma + \sqrt{\left({\eta_{r2}}^2\,\left(\theta + \theta_{r2}\right) + 2\,\gamma\right)^2 - 8\,{\eta_{r2}}^2\gamma\,\theta}\right)} \tag{45}$$

$$\xi_{NS} = \sqrt{\frac{2\,\gamma\,{\eta_{r2}}^2}{{\eta_{r2}}^2\theta_{r2} + 2\,\gamma}} \tag{46}$$

$$\xi_{NM} = \eta_{r1} \tag{47}$$

$$\text{and} \quad \xi_{IA} = \sqrt{\frac{2\,\gamma}{\theta}} \tag{48}$$

By observing the equations of ξ_1 and ξ_2, it can be concluded that they are independent of the first resonator and the mechanism of the embedded resonator in the attached inertial amplifier gives rise to two peaks (ξ_1 and ξ_2) in attenuation band. The root of the system when the second resonator is directly connected with the rigid link is given by the equation of ξ_{NS}, which is only dependant on the angle of the rigid link and second resonator. Similarly, when the first resonator is attached to main mass M, the peak in

Table 1
Closed form solution of the roots of the governing polynomials. The labels in first column corresponds to the systems given in Fig. 2(a–h).

	System	Roots of $Q=0$			Roots of $R=0$		
		q_1	q_2	q_3	r_1	r_2	r_3
a	IANMNS	ξ_1	ξ_2	ξ_{NM}	0	ζ_{r1}	ζ_{r2}
a_s	IANMNS special	ξ_1	ξ_2	–	0	ζ_{r1}	–
b	IANS	ξ_1	ξ_2	–	0	ζ_{r2}	–
c	NMNS	ξ_{NS}	ξ_{NM}	–	0	ζ_{r1}	ζ_{r2}
d	NS	ξ_{NS}	–	–	0	ζ_{r2}	–
e	IANM	ξ_{NM}	ξ_{IA}	–	0	ζ_{r1}	–
f	IA	ξ_{IA}	–	–	0	–	–
g	NM	ξ_{NM}	–	–	0	ζ_{r1}	–
h	Monoatomic	–	–	–	0	–	–

Table 2
Input data for validation.

Subsystems	M	m_a	m_1	m_2	K	k_1	k_2	$\tan\phi$
NMNS [41,49]	1	1.5	1	–	1	0.1	1	0.6
IANM [40]	1	4	2	–	1	8	–	1
NM [23,30]	0.1011	–	0.4647	–	117	74	–	–

attenuation band can be observed at ξ_{NM}, and in the case of the only inertial amplifier, the attenuation peak is developed at ξ_{IA}. It is noteworthy that the roots of the IANS system are different from the roots of the IA and NS systems, as the IANS system is the coupling of the IA and NS systems. However, when the NM system is associated with any IANS, IA, or NS system, the roots remain independent of each other as they are not coupled.

The roots of equation R are defined as following

$$\zeta_{r1} = \eta_{r1}\sqrt{(1+\theta_{r1})} \tag{49}$$

$$\text{and} \quad \zeta_{r2} = \eta_{r2} \tag{50}$$

The root ζ_{r1} is due to first resonator and ζ_{r2} is due to the second resonator.

5. Validation

The dispersion relation of few subsystems of IANMNS has been obtained in literature using different methods. The band boundaries and attenuation peaks are key features of this dispersion diagrams. In this section, the roots of equation $Q = 0$ to locate the attenuation peaks and roots of the equations $R = 0$ and $R + 2Q = 0$ to locate band boundaries has been obtained for few subsystems and validated with corresponding literature.

First, the dispersion characteristics of subsystem consists of effective negative mass negative stiffness mechanism (NMNS) has been obtained. The input parameters as per [41,49] has been chosen and given in dimensional form in Table 2. The locations of band boundaries are clearly mentioned in [41] and locations of attenuation peaks are shown in [49], which are tabulated in Table 3. The results obtained by proposed method are converted into nondimensional frequency as per the literature, and are tabulated in Table 3.

Further, the dispersion characteristics of subsystem consists of inertial amplifier with effective negative mass mechanism (IANM) has been obtained. The particular set of system parameters has been chosen (Table 2 as an example for the purpose of validation from [40]. The dispersion plot has been given in literature, from that the approximate values of dimensionless frequency has been written in Table 3. The exact analytical values has been obtained in Table 3 using the proposed method and they are written in dimensionless frequency as per literature.

Additionally, the dispersion characteristics of subsystem consists of effective negative mass mechanism (NM) has been obtained. The experimental study of a monocoupled system with negative mass mechanism has been done by [23] and that has been used for validation in [30]. The same example (Table 2) has been used here for validation. The band characteristics obtained in literature are as per Table 3. The results obtain by proposed method (Table 3) are in good agreement with the band characteristics obtain in literature.

The dispersion plot for all three subsystems has been obtained and demonstrated in Table 3.

6. Results and discussions

In this section, contour plots of attenuation levels are plotted for the generalized IANMNS system and all the other systems derived from it. The silver, blue, and green dashed lines in all the contour plots depict the roots of the equation Eq. (36), Eq. (37) and Eq. (38) respectively, which corresponds to the position of peaks in attenuation band and boundaries of dispersion diagram.

Table 3
Attenuation characteristics as per literature (lit*) and proposed (pro*) method. (For interpretation of the references to color in this table, the reader is referred to the web version of this article.)

Subsystems		NMNS		IANM		NM	
		Lit*	Pro*	Lit*	Pro*	Lit*	Pro*
Attenuation peaks	p_1	1	1	0.7	0.7071	6.3	6.351
	p_2	1.1	1.066	2	2	–	–
Band boundaries	b_1	0	0	0	0	0	0
	b_2	0.9	0.986	0.5	0.529	5.8	5.749
	b_3	1.6	1.581	2.4	2.392	7.6	7.673
	b_4	2.5	2.449	3.5	3.464	–	–
	b_5	3.9	3.873	–	–	–	–
Dispersion plot		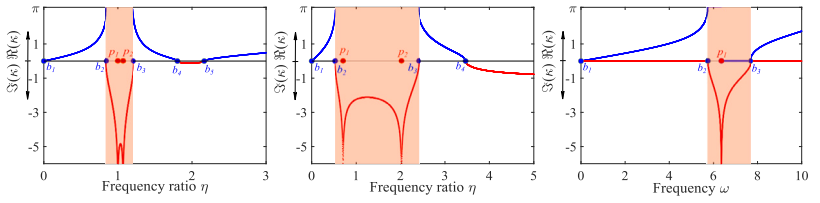					

Table 4
Systems and the values of their governing nondimensional parameters with possibility of double peak phenomenon. The labels in first column corresponds to the systems given in Fig. 2(a–h).

	System	Nondimensional parameters						Attenuation characteristics	
		θ	θ_{r1}	θ_{r2}	η_{r1}	η_{r2}	γ	Peaks	Double peak
a	IANMNS	1	3	0.25	0–5	2	1	3	Y
a_s	IANMNS special	1	3	0.25	0–5	0–5	1	2	Y
b	IANS	1	–	0.25	–	0–5	1	2	N
c	NMNS	–	3	0.25	0–5	2	1	2	Y
d	NS	–	–	0.25	–	0–5	1	1	N
e	IANM	1	3	–	0–5	–	1	2	Y
f	IA	0–5	–	–	–	–	1	1	N
g	NM	–	3	–	0–5	–	–	1	N
h	Monoatomic	–	–	–	–	–	–	0	N

The values of the governing parameters used for the analysis of each derived system are given in table Table 4. Additionally, the number of attenuation peaks in the dispersion diagram as well as the possibilities of the double peak in a single attenuation band is incorporated in Table 4.

6.1. Inertial amplifier negative mass negative stiffness (IANMNS)

Fig. 4(e) illustrates the contour of attenuation level with respect to natural frequency of mass in mass resonator (η_{r1}) and Figs. 4(a–d) illustrates the dispersion relations for particular values of η_{r1} (as shown with pink dash–dot line in Fig. 4(e)) for enhanced comprehension about the bandgap and level of attenuation within the attenuation band. In Fig. 4(a) at $\eta_{r1} = 0.5$, the roots of equations $R(\eta^2) = 0$ and $Q(\eta^2) = 0$ are occurring alternatively ($0 < \xi_{NM} < \zeta_{r1} < \xi_1 < \zeta_{r2} < \xi_2$), so the peaks in attenuation band are in separate attenuation zones. As the natural frequency of mass in mass resonator increases and crosses the value ξ_1, the positions of roots changes and the double peak phenomenon can be obtained in the first attenuation band (Fig. 4(b)). Further upon increasing η_{r1} to the value of η_{r2} the second propagation band merges and two separate peaks of attenuation band falls in a single attenuation band resulting wide band gap (Fig. 4(c)). This concludes that by having same roots of $Q = 0$ and $R = 0$ ($\xi_{NM} = \zeta_{r2}$), they will be canceled out and band merging will take place further. When $\eta_{r1} > \eta_{r2}$ the double peak will shift to the next attenuation band (Fig. 4(d)).

6.2. Inertial amplifier negative mass negative stiffness (IANMNS) special case

As it has been observed in Fig. 4(c), that by keeping both the resonators of the IANMNS system at the same frequency, the band merging will give a wide band. This phenomenon is observed in detail by varying the natural frequency of resonators from 0 to 5. The contour of attenuation level is plotted for this special case in Fig. 5(e). Figs. 5(a–d) illustrates the dispersion relation for IANMNS special case for resonators with different frequencies $\eta_{r1} = 0.5,\ 1.5,\ 2$ *and* 3.5 respectively. In Fig. 5(a) the roots position is $0 < \xi_1 < \zeta_{r1} < \xi_2$, so attenuation peaks will occur in separate attenuation bands. By increasing resonators' frequency η_{r1}, as $\zeta_{r1} > \xi_2$ the root position will shift to $0 < \xi_1 < \xi_2 < \zeta_{r1}$ which results in double peak in first attenuation band. From Fig. 5(b, c, and d), it can be observed that by increasing the frequency of the resonator, the first attenuation band gets wider, and due to the double peak phenomenon, the higher attenuation level is observed for broad frequency range.

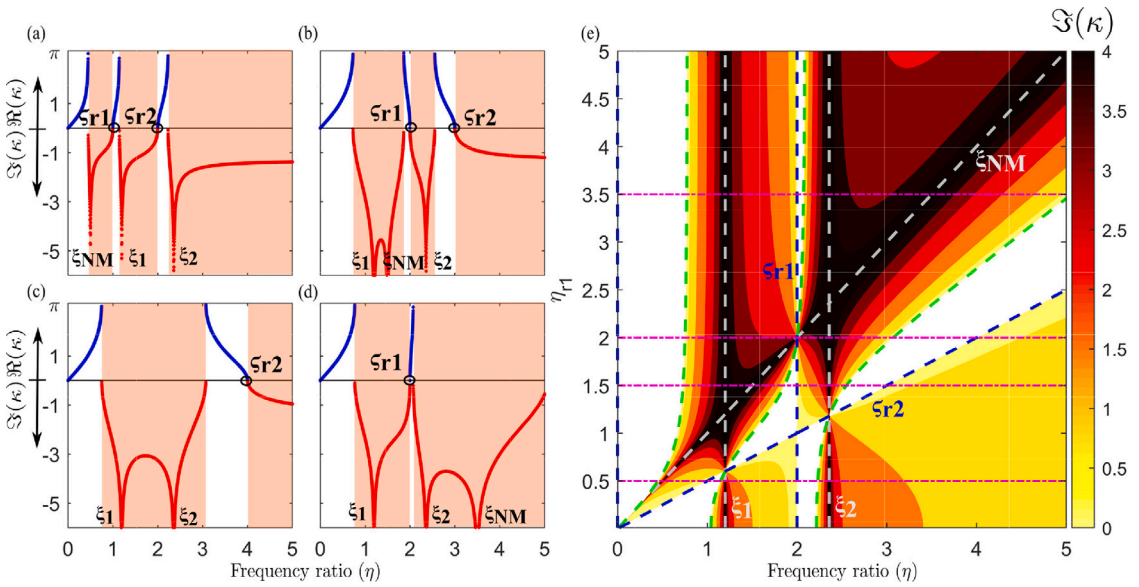

Fig. 4. The figure corresponds to IANMNS system (given in Fig. 2(a)), with values of governing parameters $\theta = 1; \theta_{r1} = 3, \theta_{r2} = 0.25, \eta_{r2} = 2, \gamma = 1$ and varying η_{r1} from 0 to 5. The contour plot for frequency ratio η varying from 0 to 5 versus η_{r1} is shown in (e). In this figure (e) the silver, blue and green dashed lines depicts the roots of equations $Q(\eta^2) = 0$, $R(\eta^2) = 0$, and $R(\eta^2) + 2\,Q(\eta^2) = 0$ respectively. The (a), (b), (c) and (d) figures demonstrates the dispersion relation for the IANMNS system at sections drawn by pink lines at $\eta_{r1} = 0.5,\ 1.5,\ 2$ *and* 3.5 respectively. (For interpretation of the references to color in this figure legend, the reader is referred to the web version of this article.)

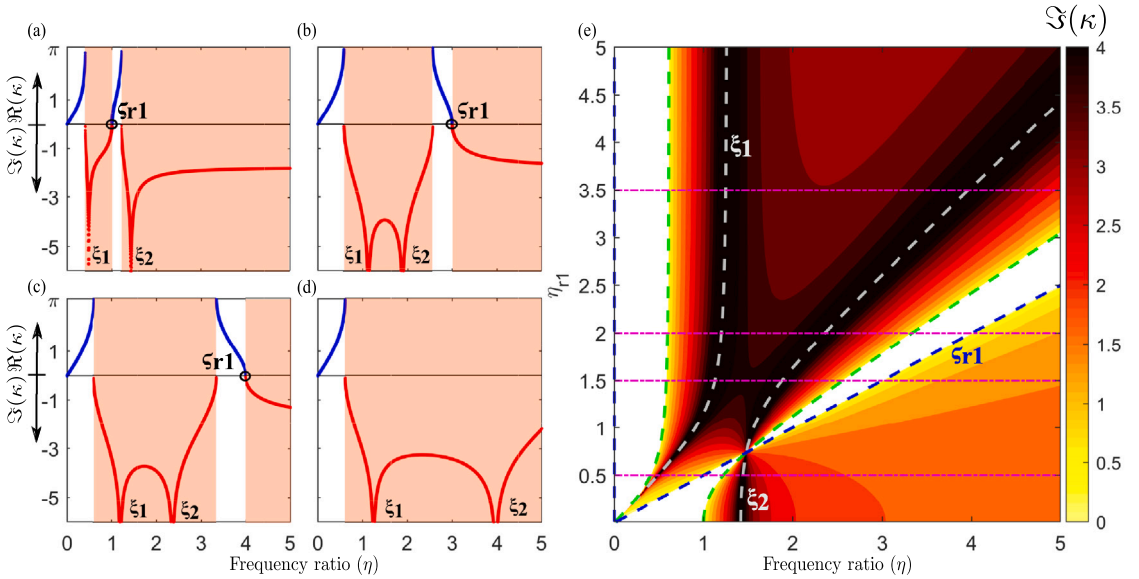

Fig. 5. IANMNS special case (with both the resonators with same frequencies ($\eta_{r1} = \eta_{r2}$)). system (given in Fig. 2(a)), with values of governing parameters $\theta = 1; \theta_{r1} = 3, \theta_{r2} = 0.25, \gamma = 1$ and varying $\eta_{r1} = \eta_{r2}$ from 0 to 5. The contour plot for frequency ratio η varying from 0 to 5 versus η_{r1} is shown in (e). In this figure (e) the silver, blue and green dashed lines depicts the roots of equations $Q(\eta^2) = 0$, $R(\eta^2) = 0$, and $R(\eta^2) + 2\,Q(\eta^2) = 0$ respectively. The (a), (b), (c) and (d) figures demonstrates the dispersion relation for the IANMNS special case system at sections drawn by pink lines at $\eta_{r1} = 0.5,\ 1.5,\ 2$ *and* 3.5 respectively. (For interpretation of the references to color in this figure legend, the reader is referred to the web version of this article.)

6.3. Negative mass negative stiffness (NMNS)

Fig. 6(e) illustrates the contour of attenuation level of NMNS system (given in Fig. 2(c)) with varying frequency of mass in mass resonator (η_{r1}) from 0 to 5. Figs. 6(a–d) illustrates the dispersion relations at natural frequencies of mass in mass resonator (η_{r1}) at 0.5, 1, 2 and 2.75 respectively. Fig. 6(a) depicts that till root $\zeta_{r1} < \xi_{NS}$, the attenuation band will have single peaks. By increasing η_{r1} further (Fig. 6(b)), the double peak in first attenuation band occurs as root $\zeta_{r1} > \xi_{NS}$. Moreover as the roots $\zeta_{r1} = \zeta_{r2}$, the merging

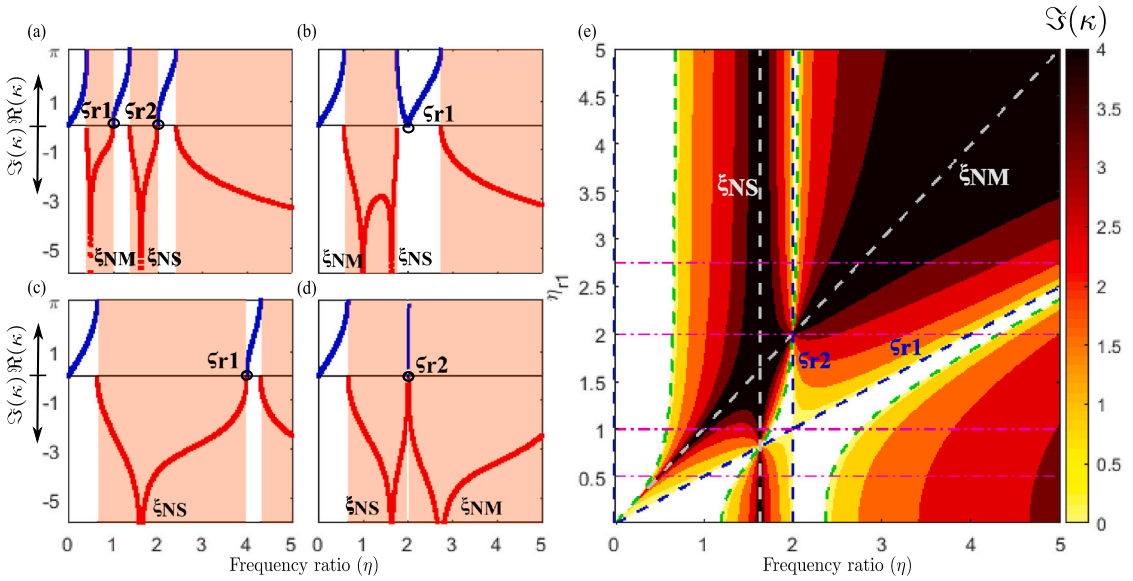

Fig. 6. NMNS system (given in Fig. 2(c)), with values of governing parameters $\theta_{r1} = 3, \theta_{r2} = 0.25, \eta_{r2} = 2, \gamma = 1$ and varying η_{r1} from 0 to 5. The contour plot for frequency ratio η varying from 0 to 5 versus η_{r1} is shown in (e). In this figure (e) the silver, blue and green dashed lines depicts the roots of equations $Q(\eta^2) = 0$, $R(\eta^2) = 0$, and $R(\eta^2) + 2\,Q(\eta^2) = 0$ respectively. The (a), (b), (c) and (d) figures demonstrates the dispersion relation for the NMNS system at sections drawn by pink lines at $\eta_{r1} = 0.5,\ 1.5,\ 2$ *and* 3.5 respectively. (For interpretation of the references to color in this figure legend, the reader is referred to the web version of this article.)

of propagation band can be observed. In Fig. 6(c), the root $\zeta_{r2} = \xi_{NM}$ results in wider attenuation band with single peak. Fig. 6(d) demonstrates that root position $\xi_{NS} < \zeta_{r2} < \xi_{NM}$ results in single peaks in attenuation bands.

6.4. Inertial amplifier negative mass (IANM)

The contour of attenuation level of IANM system (given in Fig. 2(e)) with varying frequency of mass in mass resonator (η_{r1}) from 0 to 5 is shown in Fig. 7(e). The dispersion relations at natural frequencies of mass in mass resonator (η_{r1}) at 0.5, 1, 2 and 2.75 respectively are demonstrated in Figs. 7(a–d). Fig. 7(a) depicts that till roots position is $\xi_{NM} < \zeta_{r1} < \xi_{IA}$, the attenuation band will have single peaks. By increasing η_{r1} further (Fig. 7(b)), the double peak in first attenuation band occurs as roots $\xi_{NM} < \xi_{IA} < \zeta_{r1}$. In Figs. 7(c) and (d), the root positions $\xi_{IA} < \xi_{NM} < \zeta_{r1}$ showing double peak can be observed and also the attenuation band gets wider as increase in natural frequency of mass in mass resonator.

The attenuation level contours of systems IANS (Fig. 2(b)), NS (Fig. 2(d)), IA (Fig. 2(f)), NM (Fig. 2(g)) are demonstrated in Figs 8(a), (b), (c) and (d) respectively. In IANS system, the two attenuation peaks are present but due to the coupling of IA and NS, the natural frequency of resonator always falls in between the two roots of $Q = 0$ which separates the attenuation bands Fig. 8(a). In case of NS system, the positions of attenuation peak (ξ_{NS}) and bound of propagation band (ζ_{r2}) is shown by silver and blue line in Fig. 8(b). Similarly the peak (ξ_{IA}) in attenuation band for IA is shown with silver line in Figs. 8(c) and (d) illustrates the peak (ξ_{NM}) in attenuation band and bound (ζ_{r1}) of propagation for NM system.

7. Summary

The main observations of the results are summarized as follows:

1. In the IANMNS system, a maximum three number of attenuation peaks are possible. Among them, two peaks occur due to the inertial amplifier negative stiffness (IANS) system and the third one due to the negative mass (NM) system. However, these three peaks can never be in a single attenuation band, but double peaks in a single attenuation band are possible for several cases.
2. A special IANMNS system, having both resonators with the same natural frequencies, results in a wide bandgap with double attenuation peaks due to the band merging phenomenon.
3. The IANM system also results in a wider band of high attenuation level due to double peak in the attenuation band.
4. The expressions of attenuation peaks are mainly due to the four basic mechanisms: IANS, NM, NS, and inertial amplifier (IA). The IANS system does not possess direct roots from IA and NS as they are coupled. Nevertheless, the positions of peaks in the IANM system can be directly derived from NM and IA systems as they are independent.

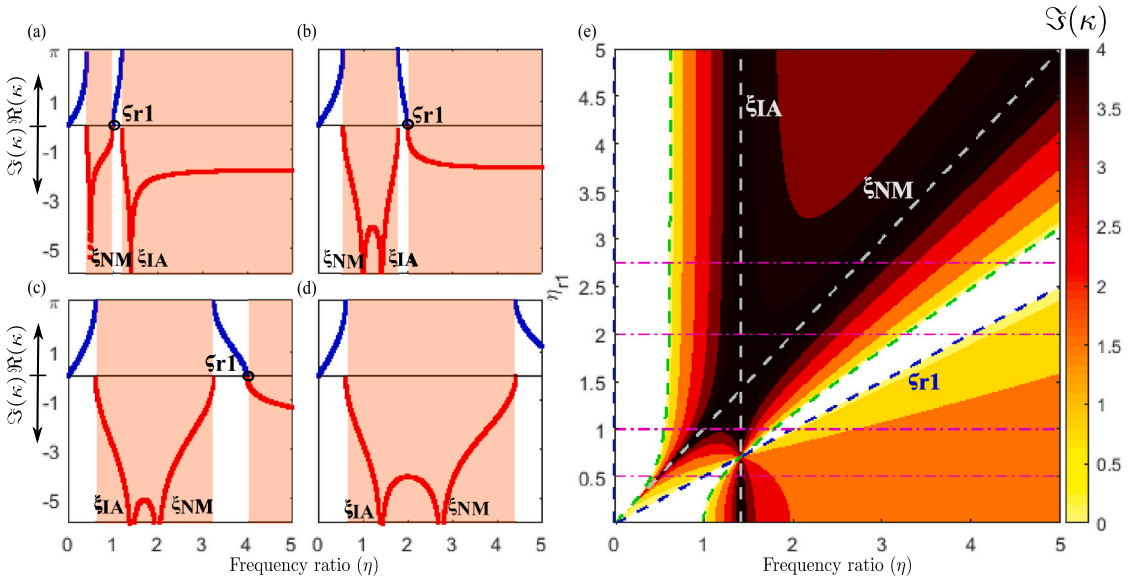

Fig. 7. IANM system (given in Fig. 2(e)), with values of governing parameters $\theta = 1$, $\theta_{r1} = 3, \gamma = 1$ and varying η_{r1} from 0 to 5. The contour plot for frequency ratio η varying from 0 to 5 versus η_{r1} is shown in (e). In this figure (e) the silver, blue and green dashed lines depicts the roots of equations $Q(\eta^2) = 0$, $R(\eta^2) = 0$, and $R(\eta^2) + 2\,Q(\eta^2) = 0$ respectively. The (a), (b), (c) and (d) figures demonstrates the dispersion relation for the IANM system at sections drawn by pink lines at $\eta_{r1} = 0.5,\ 1.5,\ 2$ *and* 2.75 respectively. (For interpretation of the references to color in this figure legend, the reader is referred to the web version of this article.)

5. While the natural frequencies of both the resonators are same $(\eta_{r1} = \eta_{r2})$, then the attenuation bands merge. On the other hand, the propagation band merges if the equation of bounds has two roots with the same values.
6. The proper tuning of the parameters of the IANMNS, negative mass negative stiffness (NMNS), and IANM systems may make them capable of obtaining double peaks in a single attenuation band. This phenomenon is desired in obtaining an attenuation bandgap with a significant attenuation level.

The overall criteria for separate attenuation peaks, double peaks phenomenon, and band merging have been illustrated for IANMNS and its seven subsystems.

8. Conclusion

In this paper, a generalized monocoupled system inertial amplifier negative mass negative stiffness (IANMNS) has been developed by coupling several different mechanisms of systems, such as an inertial amplifier, effective negative mass, and stiffness. Different types of unit cells of monocoupled systems analyzed in the literature can be obtained by assigning zero values to the specific masses.

A general theory has been developed to locate the positions and numbers of attenuation peaks as well as bounding frequencies of the propagation band of any monocoupled system using the rational polynomial equation of its dispersion relation. Exact closed-form analytical expressions for the attenuation peaks and boundaries of the dispersion diagram for the IANMNS system and seven other subsystems are obtained. Key contributions of the paper include:

- Wave propagation and dispersion equations are analyzed in several papers adopting an effective medium approach, transfer matrix approach, etc. These existing methods primarily yield the boundaries of the band, but they are unable to locate the attenuation peaks or the existence of the peak or coupling of the peaks within the attenuation band. Recently, this coupling of the attenuation peaks received very significant attention as it ensures a certain level of attenuation throughout the attenuation band. To overcome the above mentioned problem, the proposed rational polynomial approach is developed in this paper, which can locate the attenuation peaks and band boundaries. Moreover, it provides a mathematical basis for the coupling of band gaps obtained from the different band formation mechanisms.
- Perceiving a generalized inertial amplifier negative mass negative stiffness (IANMNS) monocoupled system from which seven monocoupled subsystems emerge as special cases.
- The general theory for obtaining the closed-form expressions employing the concept of roots and poles of a rational polynomial of dispersion relation has been communicated.
- The attenuation characteristics, such as bounds of the band gaps, location of the peaks in the attenuation band of the seven monocoupled subsystems, and the source, IANMNS, are compared.

Based on these findings, future monocoupled systems can be designed and specifically tuned for the required bandwidth and attenuation level by combining different mechanisms elicited in the paper.

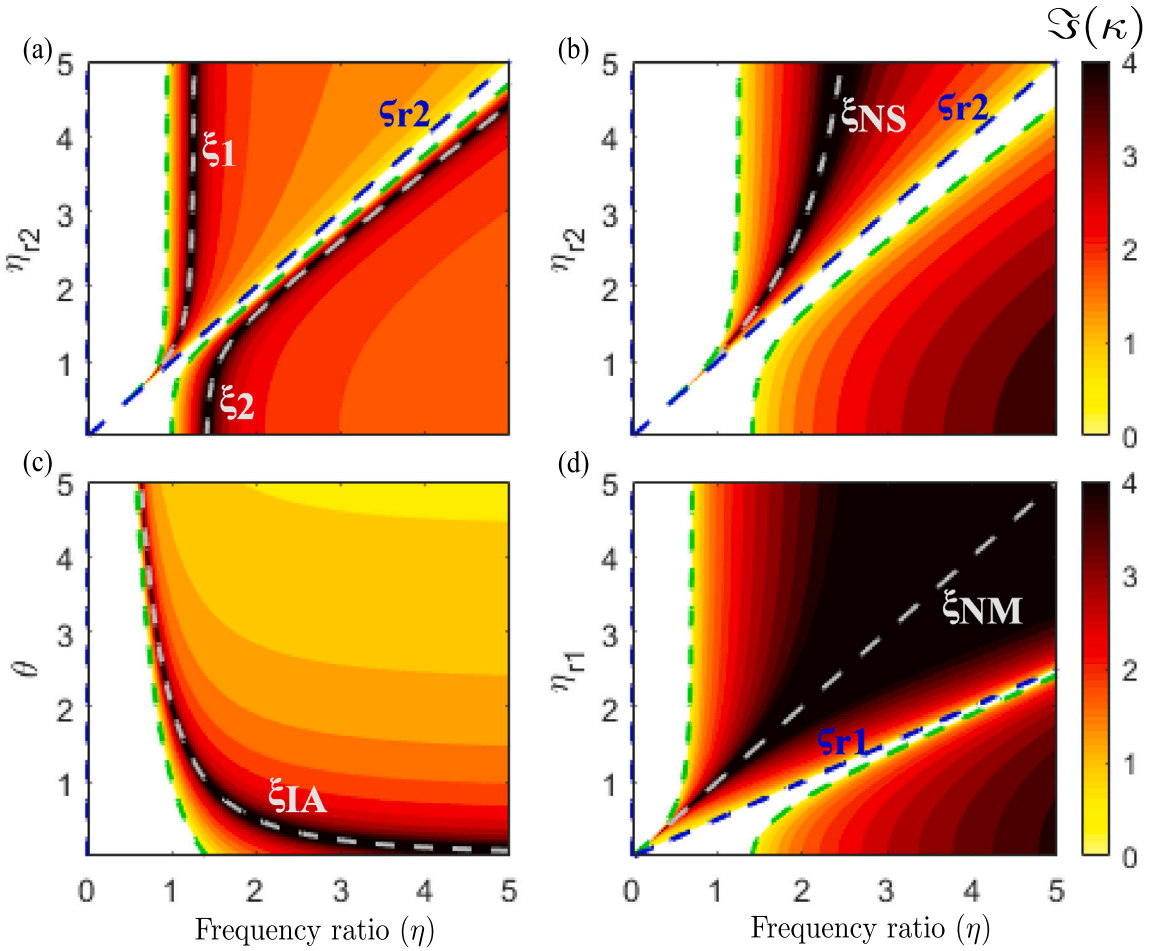

Fig. 8. (a): System—IANS (given in Fig. 2(b)), (b): System—NS (given in Fig. 2(d)), (c): System—IA (given in Fig. 2(f)), (d): System—NM (given in Fig. 2(g)), Here silver, blue and green dashed lines are roots of equations $Q(\eta^2) = 0$, $R(\eta^2) = 0$, and $R(\eta^2) + 2\,Q(\eta^2) = 0$ respectively. (For interpretation of the references to color in this figure legend, the reader is referred to the web version of this article.)

CRediT authorship contribution statement

Abhigna Bhatt: Conceptualization, Methodology, Software, Writing, Visualization, Investigation, Data curation. **Arnab Banerjee:** Conceptualization, Methodology, Review and editing, Supervision. **Sondipon Adhikari:** Conceptualization, Review and editing, Discussion, Supervision.

Declaration of competing interest

The authors declare that they have no known competing financial interests or personal relationships that could have appeared to influence the work reported in this paper.

Data availability

No data was used for the research described in the article.

Acknowledgments

Abhigna Bhatt and Arnab Banerjee acknowledge Inspire faculty award, Department of Science and Technology of India, grant number: DST/INSPIRE/04/2018/000052, for partial supporting the research.

Appendix. Roots positions of IANMNS system

The equations of roots of IANMNS system are given in Eq. (42) and Eq. (43). from roots q_1 and r_3, it can be seen that when

$$\theta_{r1} \geq 0 \quad \rightarrow \eta_{r1}\sqrt{(\theta_{r1}+1)} \geq \eta_{r1} \quad \rightarrow r_3 \geq q_1 \tag{A.1}$$

To see the positions of roots q_2 and q_3 with respect to r_2, r_2^2 is subtracted from roots q_2^2 and q_3^2

$$\begin{aligned} q_2^2 - r_2^2 &= \frac{1}{2\theta}\left(-{\eta_{r2}}^2\theta + {\eta_{r2}}^2\theta_{r2} + 2\gamma - \sqrt{\left(-{\eta_{r2}}^2\theta + {\eta_{r2}}^2\theta_{r2} + 2\gamma\right)^2 + 4{\eta_{r2}}^4\theta^2\theta_{r2}}\right) \\ q_3^2 - r_2^2 &= \frac{1}{2\theta}\left(-{\eta_{r2}}^2\theta + {\eta_{r2}}^2\theta_{r2} + 2\gamma + \sqrt{\left(-{\eta_{r2}}^2\theta + {\eta_{r2}}^2\theta_{r2} + 2\gamma\right)^2 + 4{\eta_{r2}}^4\theta^2\theta_{r2}}\right) \end{aligned} \tag{A.2}$$

Now

$$4{\eta_{r2}}^4\theta^2\theta_{r2} \geq 0 \tag{A.3}$$

$$\underbrace{\left(-{\eta_{r2}}^2\theta + {\eta_{r2}}^2\theta_{r2} + 2\gamma\right)^2}_{\chi^2} + 4{\eta_{r2}}^4\theta^2\theta_{r2} \geq \underbrace{\left(-{\eta_{r2}}^2\theta + {\eta_{r2}}^2\theta_{r2} + 2\gamma\right)^2}_{\chi^2} \tag{A.4}$$

$$\chi^2 \leq \chi^2 + 4{\eta_{r2}}^4\theta^2\theta_{r2} \tag{A.5}$$

Further it can be simplified as

$$-\sqrt{\chi^2 + 4\eta_{r2}^4\theta^2\theta_{r2}} \leq -\chi \leq \sqrt{\chi^2 + 4\eta_{r2}^4\theta^2\theta_{r2}} \tag{A.6}$$

$$\chi - \sqrt{\chi^2 + 4\eta_{r2}^4\theta^2\theta_{r2}} \leq 0 \leq \chi + \sqrt{\chi^2 + 4\eta_{r2}^4\theta^2\theta_{r2}} \tag{A.7}$$

$$\begin{aligned} &q_2^2 - r_2^2 < 0 < q_3^2 - r_2^2 \\ &q_2^2 < r_2^2 < q_3^2 \\ &q_2 < r_2 < q_3 \end{aligned} \tag{A.8}$$

From Eq. (A.8), it can be concluded that one boundary of the attenuation band lies between two attenuation peaks, which is the reason that in a single attenuation band, three attenuation peaks cannot occur.

If $r_2 < r_3$ i.e. $\eta_{r2} < \eta_{r1}\sqrt{\theta_{r1}+1}$, then root q_2 will always lie between r_1 to r_2 and root q_3 will always lie between r_2 to r_3, and as $q_1 < r_3$, this condition leads the system to have two peaks in its first attenuation band if $q_1 < r_2$ or in its second attenuation band if $q_1 > r_2$. If $r_3 < r_2$ i.e. $\eta_{r1}\sqrt{\theta_{r1}+1} < \eta_{r2}$, then first q_1 will be the peak in attenuation band, but for q_2 there are two possibilities

- $r_1 < q_2 < r_3$ double peak can be seen in first attenuation band
- $r_3 < q_2 < r_2$ double peak is not possible as $r_2 < q_3$.

References

[1] D.J. Mead, The forced vibration of one-dimensional multi-coupled periodic structures: An application to finite element analysis, J. Sound Vib. 319 (1–2) (2009) 282–304.
[2] F. Bloch, Über die quantenmechanik der elektronen in kristallgittern, Zeitschrift FÜR Physik 52 (7–8) (1929) 555–600.
[3] M.M. Sigalas, E.N. Economou, Elastic and acoustic wave band structure, J. Sound Vib. 158 (2) (1992) 377–382.
[4] L. Brillouin, Wave Propagation in Periodic Structures: Electric Filters and Crystal Lattices, Courier Corporation, 2003.
[5] J.W.S.B. Rayleigh, the Theory of Sound, Vol. 2, Macmillan, 1896.
[6] D.J. Mead, Wave propagation in continuous periodic structures: Research contributions from southampton, 1964–1995, J. Sound Vib. 190 (3) (1996) 495–524.
[7] A. Banerjee, R. Das, E. Calius, Waves in structured mediums or metamaterials: A review, Arch. Comput. Methods Eng. 26 (4) (2019).
[8] Y. Lu, F. Wang, X. Ma, Helicopter interior noise reduction using compounded periodic struts, J. Sound Vib. 435 (2018) 264–280.
[9] K.K. Reichl, D.J. Inman, Lumped mass model of a 1D metastructure for vibration suppression with no additional mass, J. Sound Vib. 403 (2017) 75–89.
[10] O. Abdeljaber, O. Avci, D.J. Inman, Optimization of chiral lattice based metastructures for broadband vibration suppression using genetic algorithms, J. Sound Vib. 369 (2016) 50–62.
[11] D.J. Mead, Plates with regular stiffening in acoustic media: vibration and radiation, J. Acoust. Soc. Am. 88 (1) (1990) 391–401.
[12] L. D'Alessandro, E. Belloni, R. Ardito, A. Corigliano, F. Braghin, Modeling and experimental verification of an ultra-wide bandgap in 3D phononic crystal, Appl. Phys. Lett. 109 (22) (2016) 221907.
[13] M.S. Kushwaha, P. Halevi, L. Dobrzynski, B. Djafari-Rouhani, Acoustic band structure of periodic elastic composites, Phys. Rev. Lett. 71 (13) (1993) 2022.
[14] V. Laude, Phononic crystals: Artificial crystals for sonic, in: Acoustic and Elastic Waves Berlin, De Gruyter, 2015.
[15] M.I. Hussein, M.J. Leamy, M. Ruzzene, Dynamics of phononic materials and structures: Historical origins, recent progress, and future outlook, Appl. Mech. Rev. 66 (4) (2014).
[16] Z. Liu, X. Zhang, Y. Mao, Y.Y. Zhu, Z. Yang, C.T. Chan, P. Sheng, Locally resonant sonic materials, Science 289 (5485) (2000) 1734–1736.
[17] Y. Xiao, B.R. Mace, J. Wen, X. Wen, Formation and coupling of band gaps in a locally resonant elastic system comprising a string with attached resonators, Phys. Lett. A 375 (12) (2011) 1485–1491.
[18] A.O. Krushynska, V.G. Kouznetsova, M.G. Geers, Towards optimal design of locally resonant acoustic metamaterials, J. Mech. Phys. Solids 71 (2014) 179–196.
[19] F. Casadei, K. Bertoldi, Wave propagation in beams with periodic arrays of airfoil-shaped resonating units, J. Sound Vib. 333 (24) (2014) 6532–6547.

[20] S. Krödel, N. Thomé, C. Daraio, Wide band-gap seismic metastructures, Extrem. Mech. Lett. 4 (2015) 111–117.
[21] C. Sugino, S. Leadenham, M. Ruzzene, A. Erturk, On the mechanism of bandgap formation in locally resonant finite elastic metamaterials, J. Appl. Phys. 120 (13) (2016) 134501.
[22] E.P. Calius, X. Bremaud, B. Smith, A. Hall, Negative mass sound shielding structures: Early results, Phys. Status Solidi b 246 (9) (2009) 2089–2097.
[23] S. Yao, X. Zhou, G. Hu, Experimental study on negative effective mass in a 1D mass–spring system, New J. Phys. 10 (4) (2008) 43020.
[24] H. Huang, C. Sun, G. Huang, On the negative effective mass density in acoustic metamaterials, Internat. J. Engrg. Sci. 47 (4) (2009) 610–617.
[25] H. Huang, C. Sun, Theoretical investigation of the behavior of an acoustic metamaterial with extreme Young's modulus, J. Mech. Phys. Solids 59 (10) (2011) 2070–2081.
[26] L. Sam Hyeon, P. Choon Mahn, S. Yong Mun, W. Zhi Guo, K. Chul Koo, Acoustic metamaterial with negative modulus, J. Phys.: Condens. Matter 21 (17) (2009) 175704.
[27] E. Pasternak, A.V. Dyskin, G. Sevel, Chains of oscillators with negative stiffness elements, J. Sound Vib. 333 (24) (2014) 6676–6687.
[28] I.-L. Chang, Z.-X. Liang, H.-W. Kao, S.-H. Chang, C.-Y. Yang, The wave attenuation mechanism of the periodic local resonant metamaterial, J. Sound Vib. 412 (2018) 349–359.
[29] X. Xu, M.V. Barnhart, X. Li, Y. Chen, G. Huang, Tailoring vibration suppression bands with hierarchical metamaterials containing local resonators, J. Sound Vib. 442 (2019) 237–248.
[30] A. Banerjee, R. Das, E.P. Calius, Frequency graded 1D metamaterials: a study on the attenuation bands, J. Appl. Phys. 122 (7) (2017) 075101.
[31] D.R. Smith, W.J. Padilla, D.C. Vier, S.C. Nemat-Nasser, S. Schultz, Composite medium with simultaneously negative permeability and permittivity, Phys. Rev. Lett. 84 (18) (2000) 4184–4187.
[32] C. Yilmaz, G.M. Hulbert, N. Kikuchi, Phononic band gaps induced by inertial amplification in periodic media, Phys. Rev. B 76 (5) (2007) 054309.
[33] M.C. Smith, Synthesis of mechanical networks: the inerter, IEEE Trans. Automat. Control 47 (10) (2002) 1648–1662.
[34] S. Chowdhury, A. Banerjee, S. Adhikari, Enhanced seismic base isolation using inertial amplifiers, in: Structures, Vol. 33, Elsevier, 2021, pp. 1340–1353.
[35] N.M.M. Frandsen, O.R. Bilal, J.S. Jensen, M.I. Hussein, Inertial amplification of continuous structures: Large band gaps from small masses, J. Appl. Phys. 119 (12) (2016) 124902.
[36] A.H. Orta, C. Yilmaz, Inertial amplification induced phononic band gaps generated by a compliant axial to rotary motion conversion mechanism, J. Sound Vib. 439 (2019) 329–343.
[37] K. Mizukami, K. Funaba, K. Ogi, Design and three-dimensional printing of carbon-fiber-composite elastic metamaterials with inertial amplification mechanisms, J. Sound Vib. 513 (2021) 116412.
[38] Y. Gao, L. Wang, Ultrawide coupled bandgap in hybrid periodic system with multiple resonators, J. Appl. Phys. 127 (20) (2020) 204901.
[39] A. Stein, M. Nouh, T. Singh, Widening, transition and coalescence of local resonance band gaps in multi-resonator acoustic metamaterials: From unit cells to finite chains, J. Sound Vib. (2022) 116716.
[40] A. Banerjee, S. Adhikari, M.I. Hussein, Inertial amplification band-gap generation by coupling a levered mass with a locally resonant mass, Int. J. Mech. Sci. 207 (2021) 106630.
[41] H.-H. Huang, C.-T. Sun, Anomalous wave propagation in a one-dimensional acoustic metamaterial having simultaneously negative mass density and Young's modulus, J. Acoust. Soc. Am. 132 (4) (2012) 2887–2895.
[42] J. Li, C.T. Chan, Double-negative acoustic metamaterial, Phys. Rev. E 70 (5) (2004) 55602.
[43] P.L. Marston, Comment on " anomalous wave propagation in a one- dimensional acoustic metamaterial having simultaneously negative mass density and Young's modulus" [j. Acoust. Soc. Am. 132, 2887-2895 (2012)], J. Acoust. Soc. Am. 135 (3) (2014) 1031–1033.
[44] A. Baxy, R. Prasad, A. Banerjee, Elastic waves in layered periodic curved beams, J. Sound Vib. 512 (2021) 116387.
[45] C. Sugino, Y. Xia, S. Leadenham, M. Ruzzene, A. Erturk, A general theory for bandgap estimation in locally resonant metastructures, J. Sound Vib. 406 (2017) 104–123.
[46] S.-L. Yeh, R.L. Harne, Origins of broadband vibration attenuation empowered by optimized viscoelastic metamaterial inclusions, J. Sound Vib. 458 (2019) 218–237.
[47] M.I. Hussein, I. Patrick, A. Banerjee, S. Adhikari, Metadamping in inertially amplified metamaterials: Trade-off between spatial attenuation and temporal attenuation, J. Sound Vib. 531 (2022) 116977.
[48] D.J. Mead, Wave propagation and natural modes in periodic systems: I. mono-coupled systems, J. Sound Vib. 40 (1) (1975) 1–18.
[49] A. Bhatt, A. Banerjee, Double attenuation peaks in metamaterial with simultaneous negative mass and stiffness, Phys. Lett. A (2022) 128201.